Electronic Supplementary Material (ESI) for ChemComm.

Supplemental

Support effects in the adsorption of water on CVD graphene: an ultra-high vacuum adsorption study

A. Chakradhar, N. Sivapragasam, Mindika Tilan Nayakasinghe, and U. Burghaus

Department of Chemistry and Biochemistry,
North Dakota State University, Fargo, USA

www.uweburghaus.us

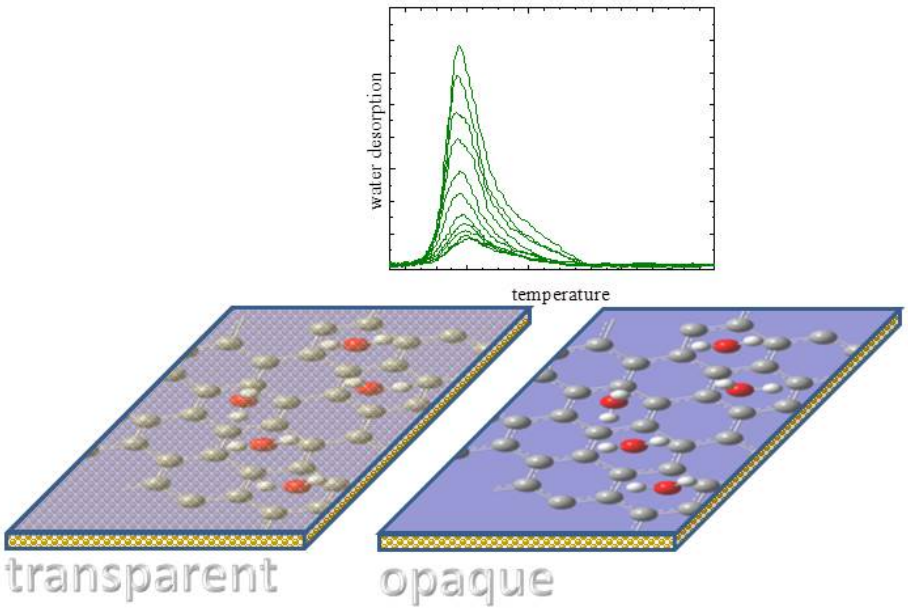

Wetting properties can be identified using ultra-high vacuum thermal desorption spectroscopy

Hydrophobic systems				
System	**Hydro-phobic**	**0th order**	**TDS peaks**	**Ref.**
Au(111)	Yes	Yes	1	[1]
Antimony(111)	Yes	Yes	1	[2]
Cu(111)	Yes	Yes	1	[3]
O_2-Au(111)	Yes	Yes	1	[4]
D_2-Ni(111)	Yes	Yes	1	[5]
D_2-Pt(533)	Yes	Yes	1	[6]
Octane-Pt(111)	Yes	Yes	1	[7]
Water-Pt(111)	Yes	Yes	1	[8]
Hydrophilic systems				
Ru(0001)	No	No	3	[9]
JSC-A1	No	No	5	[10]
TiO_2(110)	No	No	3	[11]
Pt(111)	No	No	2	[8]

Tab. S1: UHV (ultra-high vacuum) kinetics experiments of water on several surfaces.

A list of hydrophobic and hydrophilic surfaces that have been studied in surface science are listed in Tab. S1. As evident, TDS (thermal desorption spectroscopy) clearly allows for distinguishing the wetting properties of surfaces. In addition, as an ultra-high vacuum technique, TDS characterizes the intrinsic properties of the surfaces. Au(111) and Sb(111) are probably the clearest examples of hydrophobic single crystal systems. Copper is trickier, as it exhibits both hydrophobic and hydrophilic properties depending on the crystallographic orientation of the surface. Polycrystalline copper was apparently not studied before. Therefore, we characterized the polycrystalline Cu foil (exact support used to grow graphene) in blind experiments (see below). Accordingly, the polycrystalline Cu foil is hydrophilic in nature.

Sample characterization

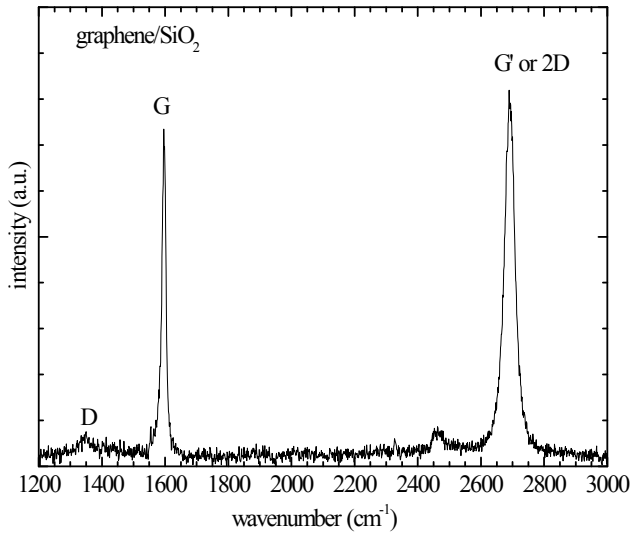

Fig. S1: Raman spectrum of graphene/SiO_2 taken before mounting the sample in UHV.

The Raman spectrum for as-received graphene/SiO_2 is shown in **Fig. S1**. which is indicative of a small defect density, as represented by the small D peak intensity. The intensity of the D-peak is proportional to the amount of disorder in the sample. The ratio between the intensities of the disorder-induced D-band (I_D) and the first-order graphite G-band (I_G) can be used for quantifying disorder in the sample. The ratio of I_D to I_G lines corresponds to only ~0.08, therefore; the graphene samples studied in this project are of appropriate quality.

Furthermore, spectroscopy can in principle distinguish between amorphous and crystalline carbon as well as other contaminations. For example, XPS chemical shifts are, however, in practice demanding to analyze precisely due to uncertainties in the calibration of the energy scale. Therefore, we collected additionally Raman spectra. Our Raman data are consistent with graphene. Raman spectra of amorphous carbon look quite different than our Raman spectra from graphene, see e.g. ref. [Mildred S. Dresselhaus, Ado Jorio, Mario Hofmann, Gene Dresselhaus, and Riichiro Saito, Nano Lett. **2010,** 10, 751–758]. Therefore, we can at least rule out large amounts of amorphous carbon contaminations.

See also section about sample cleanliness below.

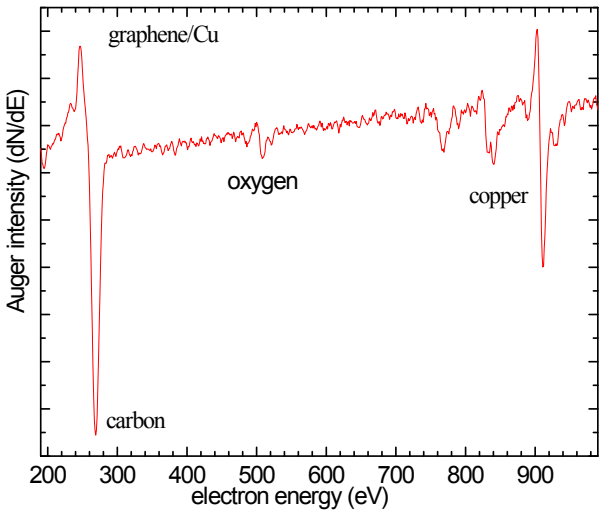

Fig. S2A: Auger electron spectrum of as received graphene/Cu.

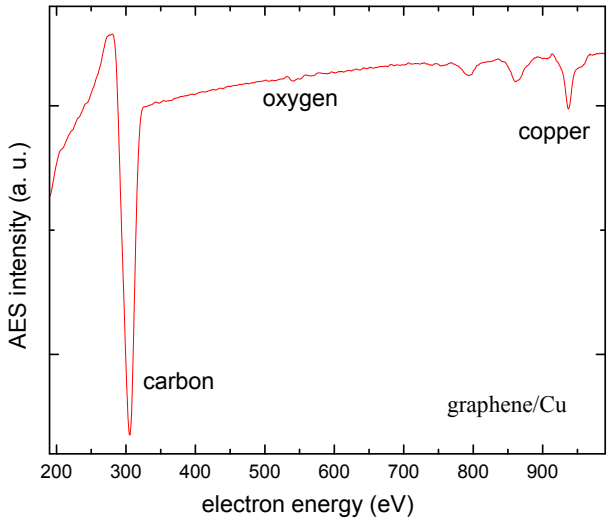

Fig. S2B: Auger electron spectrum of as received graphene/Cu. (Different sample as shown in A.)

Fig. S2 depicts Auger spectra for the as-received CVD graphene/Cu samples. A peak at ~271 eV and peaks at higher energies correspond to carbon (from graphene), and copper (from support), respectively. See also section about surface cleanliness below.

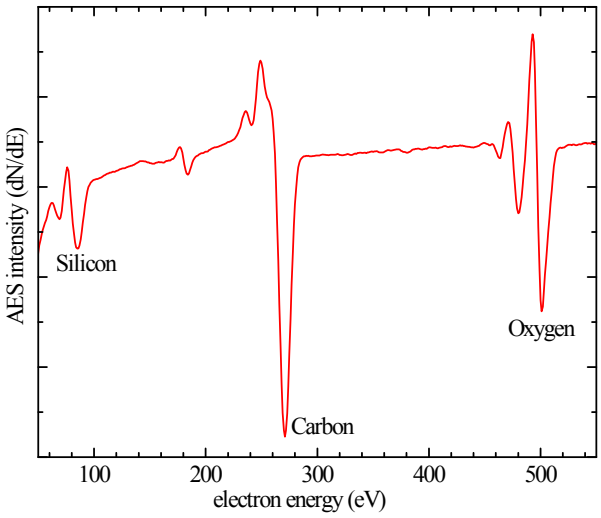

Fig. S3: Auger electron spectrum of as-received graphene/SiO_2.

Fig. S3 depicts an Auger spectrum for the as-received CVD graphene/SiO_2 sample. A peak at ~80 eV, a peak at ~271 eV, and a peak at ~503 eV correspond to silicon (from support), carbon (from graphene), and oxygen (from support), respectively.

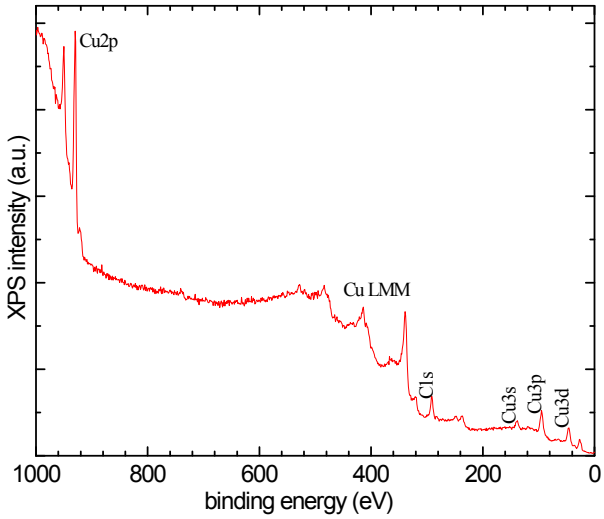

Fig. S4: XPS survey of graphene/Cu.

X-ray photoelectron spectroscopy survey scan for the as-received CVD graphene/Cu sample is depicted in **Fig. S4.** For XPS, a Mg Kα line (at 1253.6 eV) was used with a pass-energy of 50 eV of the analyzer.

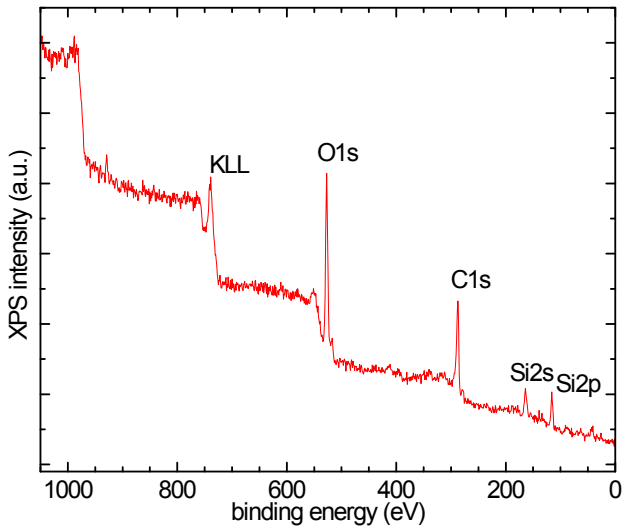

Fig. S5: XPS survey of graphene/SiO_2.

X-ray photoelectron spectroscopy survey scan for the as-received CVD graphene/SiO_2 is depicted in **Fig. S5.**

Sample cleanliness

Some notes about sample cleanliness were already given above and in the draft. Shortly after the first studies on graphene this issue became, however, of concern, see e.g. ref.[12] Therefore, we added mode details here.

- We looked at more than one sample. The O-AES peak intensity varied somewhat from sample to sample (Fig. S2A/B).
- We also looked at blank samples, i.e., just the copper foil. In that case an O-AES peak was already present (see Fig. S8). Thus, the O-AES signal is unlikely intrinsic to the graphene.
- For graphene/copper, we also collected XPS of the copper region (see Fig. S9) with greater resolution than for the XPS survey scans. In that case, we saw a satellite peak in XPS which is characteristic of an oxide. Thus, the Cu CVD graphene samples are more precisely described as graphene/CuO_x samples. We attribute the O-AES peak to the copper oxide support. The copper blanks already show the oxide satellite peak.
- The variations seen in the O-AES peak intensities on different samples may be related to the samples' history, as noted on the website of the vendor. It appears that the Cu support oxidizes over time. Smaller XPS satellite peaks for the graphene samples as compared with the Cu blank are related to screening effects.
- We did flash the graphene samples to the greatest possible temperature in UHV to clean off eventual oxygen functionalities. Even larger flash/annealing temperature damaged the samples. (The graphene basically disappeared according to XPS/AES. Probably dissolved in the bulk of the sample.)

In summary, we can write with confidence that the samples studied here are among the cleaning CVD samples studied so far. Although model systems such as graphene/Ruthenium (directly made in the UHV[13]) will be cleaner, basically the same CVD samples were used in a variety of other studies including engineering type works. Therefore, our UHV CVD work may act as a reference studying the cleanest possible CVD graphene samples in UHV.

Additional Data

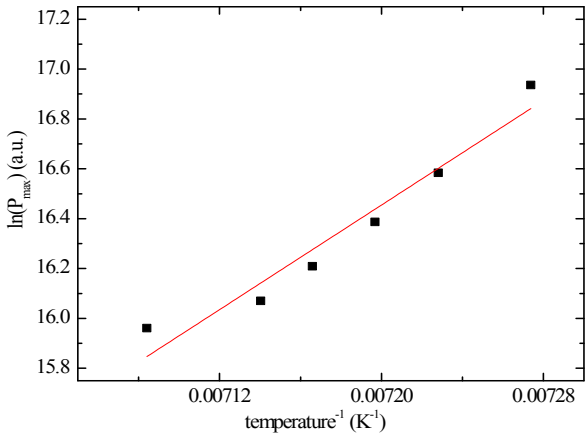

Fig. S6: Kinetics parameter for water adsorption on graphene/SiO_2.

The Arrhenius plot for water adsorption on graphene/SiO_2 at lower exposures is depicted in **Fig. S6.** It is a straight line, but with a positive slope. For zero-order kinetics, a negative slope would be expected. Therefore, graphene/SiO_2 is hydrophilic as also evident from the shape of the TDS curves.

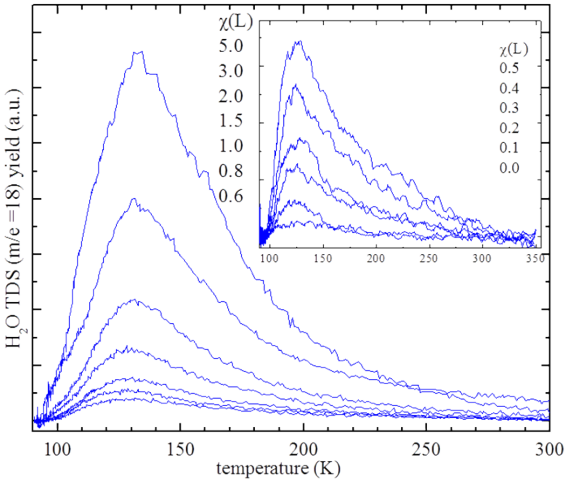

Fig. S7: Thermal desorption data of water on the Cu support as a function of water exposure. Inset shows data for low exposures.

Fig. S7 depicts a single broad TDS feature for adsorption of water on the polycrystalline Cu support. The low temperature leading edges of the TDS curves do not align (hydrophilic system). Therefore, the kinetics deviates from zero-order kinetics which is expected for a hydrophilic system.

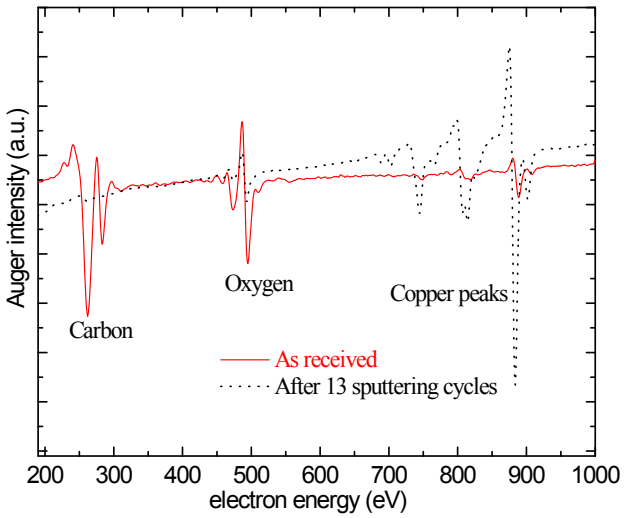

Fig. S8: AES data of a copper blank sample. The exact same type of copper foil used for the CVD process was used here. The copper foil was cleaned in UHV by sputtering before collecting blind experiments. The residual oxygen peak is likely related to a surface oxide.

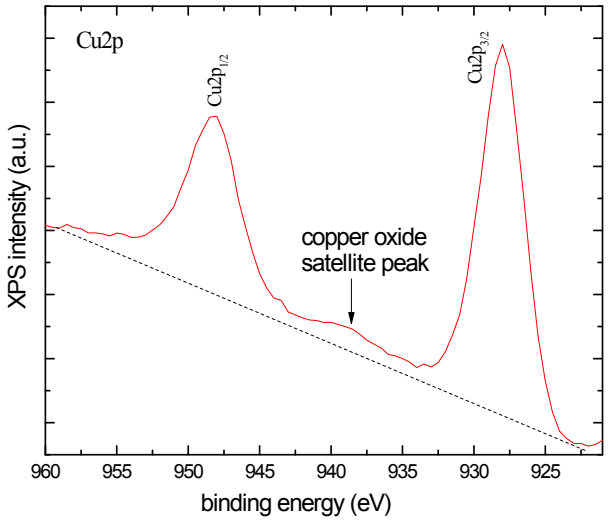

Fig. S9A: XPS data of the copper region for a graphene/copper sample.

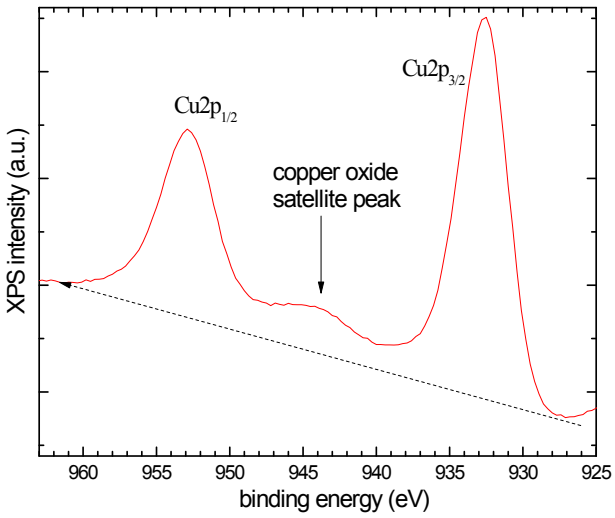

Fig. S9B: XPS data of the copper region for a copper foil blank sample.

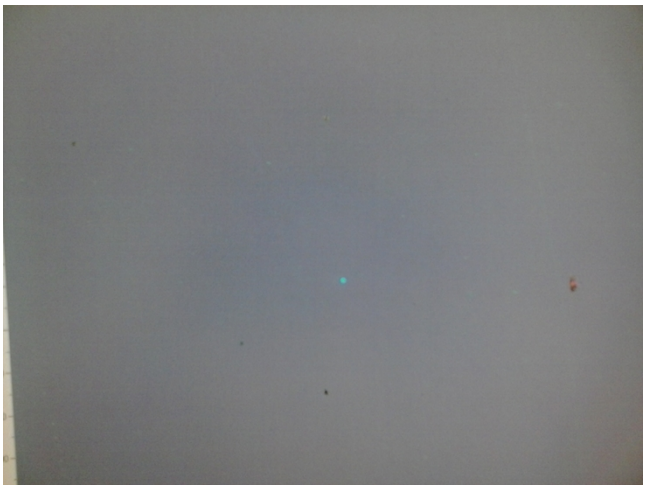

Fig. S10: Micrograph collected with an optical microscope for a graphene sample studied here.

Data analysis for Fig. 2 of the draft (desorption energy calculation)

Fig. 2 in the main draft was obtained using the following standard data analysis procedure. For strictly zero-order kinetics the desorption rate, k, is simply described by an Arrhenius equation, according to:

$$k = k_d[A_{ads}]^0 = k_d;$$
$$\mathrm{k_d} = \nu_d e^{-E_b/RT};$$
$$\ln(k_d) = \ln(\nu_d) - E_b / R\frac{1}{T} \text{ or}$$
$$\ln(k_d) = \ln(\nu_d) - E_b / k_b\frac{1}{T}$$

where,

k_d is the desorption rate coefficient,

ν is the pre-exponential coefficient,

E_b is the binding energy (here sublimation energy of water),

T is the surface temperature,

$[A_{ads}]$ or Θ is the adsorbate coverage/concentration,

R is the gas constant,

k_b is the Boltzmann constant.

The desorption rate is coverage independent. We can rewrite the above equations as,

$$\beta\frac{d\Theta}{dT} = k_d = \nu e^{-E/RT}$$
$$\beta r = \nu e^{-E/RT}$$
$$r = \nu/\beta\, e^{-E/RT}$$
$$\ln(r) = \ln(\nu/\beta) - E / RT$$

β represents the heating rate in this equation. TDS measures the pressure of the desorbing adsorbates, or, equivalent to that, the change of coverage (surface concentration) which is given by dΘ/dT. The change of coverage with temperature equals the desorption rate, r. The desorption rate is proportional to the measured pressure (i.e. the TDS peak intensity).

Fig. 2 shows this kind of data analysis. The TDS peak positions (in Kelvin) are plotted against the TDS peak intensity. The TDS data set of **Fig. 1** in the main draft was used. The slope of the fit line gives the heat of sublimation of water (see equations above). In doing so, numerical values very close to the heat of sublimation of water were obtained, another indication for simple condensation kinetics of water on graphene.

Similarly, for the inset of **Fig. 2** in the main draft, the 6L TDS curve was considered to obtain the heat of condensation of water by leading edge method. The plot of the logarithm of desorption rate vs. inverse of temperature (K^{-1}) yielded a straight line. The slope of this line was used to calculate desorption energy by utilizing previously mentioned equation. As a result, a heat of condensation value of 0.46 eV/molecule was obtained, which is consistent with the water condensation value (0.49eV/molecule).[14]

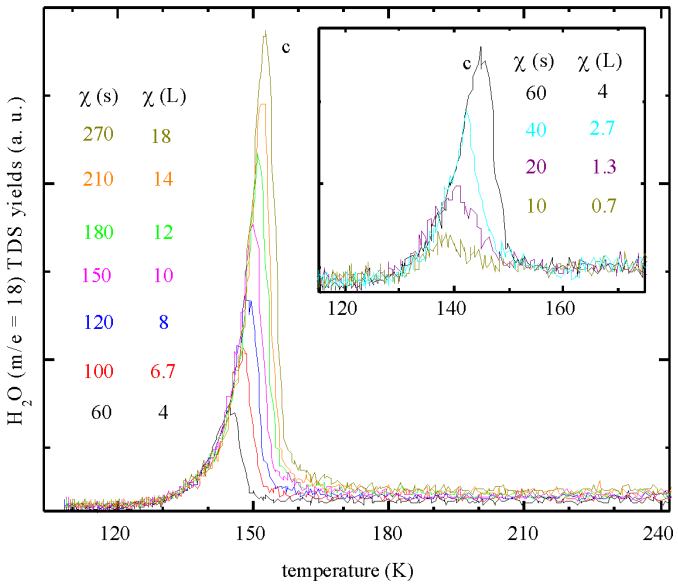

Fig. S11: Example of a strict zero-order kinetics data set taken in the same experimental set up – see *Adsorption of water on a hydrophobic surface - the case of antimony(111),* Chem. Phys. Lett., 517 (2011) 46-50, by J. Shan, A. Chakradhar, Z. Yu, U. Burghaus

Fig. S11 shows an example of TDS curves on a hydrophobic surface obtained with the same UHV set up, which shows an abruptly sharp drop in the desorption rate at higher temperature. Sb(111) is one of the single crystal systems, which clearly shows hydrophobic properties. Here, indeed a sharp drop of the signal is evident for the high temperature edges of the TDS curves. Therefore, pumping speed effects and readsorption can be ruled out in our UHV system. We conclude that the high temperature TDS feature, observed in our study, is intrinsic to graphene/Cu and indicated a deviation from exact zero-order kinetics.

Experimental setup

The measurements have been performed with the UHV system shown in **Fig. S12**.[15] The base pressure of the scattering chamber was in the low 10^{-10} mbar range. The UHV system contains a shielded mass spectrometer for thermal desorption spectroscopy (TDS) as well as an AES (Auger electron spectroscopy) and XPS (X-ray photoelectron spectroscopy) spectrometer.

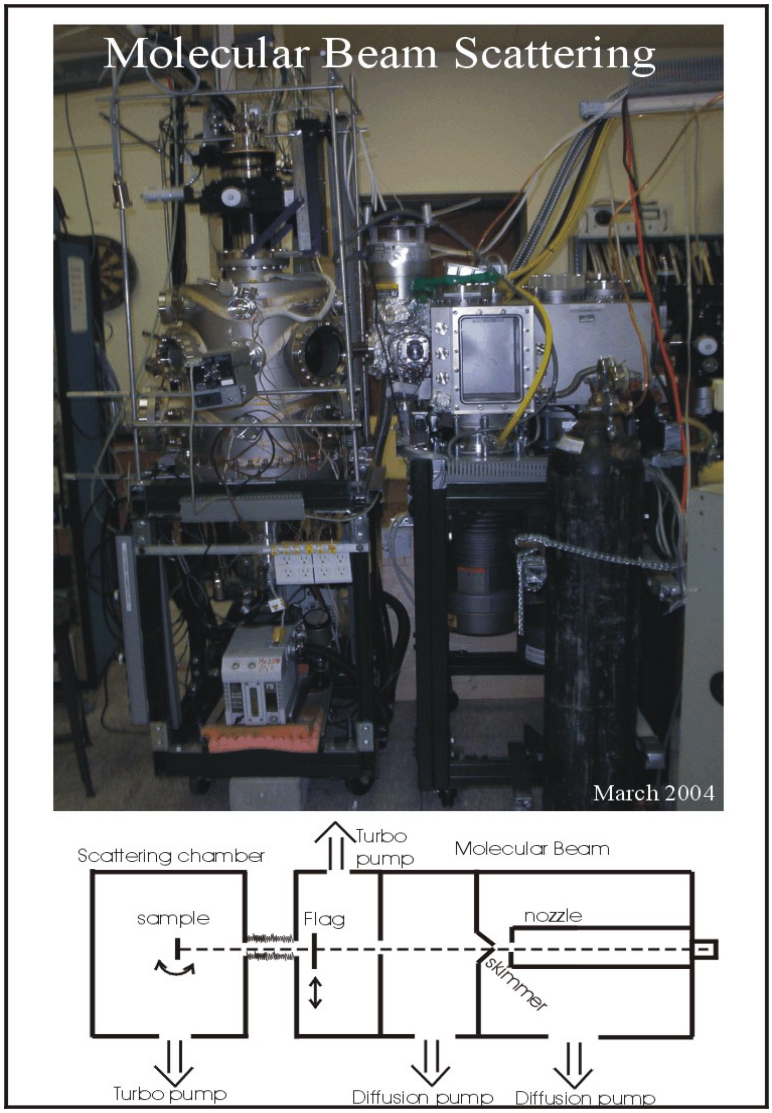

Fig. S12: Set-up of the molecular beam scattering chamber.

Thermal desorption spectroscopy

Thermal desorption spectroscopy (TDS), also known as temperature programmed desorption (TPD), is an important technique to determine the kinetic and thermodynamic parameters of desorption processes and decomposition reactions. The sample is mounted inside a UHV vacuum chamber. The sample is initially maintained at cryogenic temperature. A desired gas molecule is exposed to the clean surface; that way the adsorbed molecule is bound to the surface in a potential well of depth E_{des}. Then, this adsorbed gas molecule/atom is desorbed by heating the surface. The pressure rise is monitored and the desorbed gas molecules are detected by a quadruple mass spectrometer.

In principle, we can get information about heat of adsorption whether adsorption and desorption are reversible/non-dissociative processes, quantitative coverage information of dissociative and non-dissociative adsorption, energetic information about the interadsorbate interactions, several adsorption sites, and kinetic information about desorption processes and decomposition reactions.

TDS spectra depict simply the pressure of a given gaseous molecule vs. surface temperature. This pressure is related to the desorption rate. Thus, we obtain kinetics information since the higher the peak temperature the larger the binding energy of the probe molecule on the surface. Integrating the TDS curves quantifies the total amount of adsorbed species.

References

(1) Kay, B. D.; Lykke, K. R.; Creighton, J. R.; Ward, S. J. *J.Chem.Phys.* **1989**, *91*, 5120.
(2) Shan, J.; Chakradhar, A.; Yu, Z.; Burghaus, U. *Chem. Phys. Lett.* **2011**, *517*, 46.
(3) Hinch, B. J.; Dubois, L. H. *J. Chem. Phys.* **1992**, *96*, 3262.
(4) Quiller, R. G.; Baker, T. A.; Deng, X.; Colling, M. E.; Min, B. K.; Friend, C. M. *J. Chem. Phys.* **2008**, *129*, 064702
(5) Shan, J.; Aarts, J. F. M.; Kleyn, A. W.; Juurlink, L. B. F. *Phys. Chem. Chem. Phys.* **2008**, *10*, 4994.
(6) Niet, M. J. T. C. v. d.; Dominicus, I.; Koper, M. T. M.; Juurlink, L. B. F. *Phys. Chem. Chem. Phys.* **2008**, *10*, 7169.
(7) Linderoth, T. R.; Zhdanov, V. P.; Kasemo, B. *Phys. Rev. Lett.* **2003**, *90*, 156103.

(8) Kimmel, G. A.; Petrik, N. G.; Dohnalek, Z.; Kay, B. D. *Phys. Rev. Lett.* **2005**, *95*, 166102
(9) Polta, J. A.; Thiel, P. A. *J. Am. Chem. Soc.* **1986**, *108*, 7560.
(10) Goering, J.; Sah, S.; Burghaus, U.; Street, K. W. *Surface and Interface Analysis* **2008**, *40*, 1423.
(11) Brinkley, D.; Dietrich, M.; Engel, T.; Farrall, P.; Ganter, G.; Schafer, A.; Szuchmacher, A. *Surface Science* **1998**, *395*, 292.
(12) Li, Z.; Wang, Y.; Kozbial, A.; Shenoy, G.; Zhou, F.; McGinley, R.; Ireland, P.; Morganstein, B.; Kunkel, A.; Surwade, S. P.; Li, L.; Liu, H. *Nature Mat.* **2013**, 925.
(13) Chakradhar, A.; Burghaus, U. *Chemical Communications* **2014**, *50*, 7698.
(14) Chakarov, D. V.; Osterlund, L.; Kasemo, B. *Vacuum* **1995**, *46*, 1109.
(15) Wang, J.; Burghaus, U. *Journal of Chemical Physics* **2005**, *123*, 184716.

Funding Source

The donors of the American Chemical Society and Petroleum Research Fund are acknowledged for partial financial support.

Generic list of acronyms and abbreviations

AES	Auger electron spectroscopy
AFM	atomic force microscopy
CMA	cylindrical mirror analyzer
CNTs	carbon nanotubes
CVD	chemical vapor deposition
DFT	density functional theory
EBL	electron beam lithography
EDX/EDS	energy dispersive X-ray spectroscopy
GC	gas chromatograph
HDS	hydrodesulfurization
HREELS	high resolution electron energy loss spectroscopy
IF	inorganic fullerene-like nanoparticles
LEED	low energy electron diffraction
MBRS	molecular beam relaxation spectroscopy
MCS	Monte Carlo simulations
NDSU	North Dakota State University
NT	nanotubes
NP	nanoparticles
PNNL	Pacific Northwest National Laboratory
PVD	physical vapor deposition
SEM	scanning electron microscopy
STM	scanning tunneling microscopy
TEM	transmission electron microscopy
TiNTs	TiO_2 nanotubes
TDS	thermal desorption spectroscopy
TOF	time of flight spectroscopy
UHV	ultra-high vacuum
UPS	ultraviolet photoelectron spectroscopy
UV	ultraviolet
XPS	x-ray photoelectron spectroscopy